An Overloaded Pure Silica Zeolite ISV Synthesized Using a Phosphonium Cation

Huajian Yu, Salvador R. G. Balestra, Zihao Rei Gao, Miguel A. Camblor

Supplementary information

1. Details of the calculation methods and software
2. Construction of crystalline materials
3. Structural Characterization
4. Figures

1. Details of the calculation methods and software

Energy optimisation methods

We performed periodic fully flexible optimizations (*i.e.*, optimizing all atom coordinates and lattice parameters, without considering symmetry) using three theoretical levels: DFT, TB, and classical force field.

1. **r^{2}SCAN+rVV10 (electronic structure) method**: We used the meta-GGA r^{2}SCAN exchange-correlation functional of Furness *et al.*,[1] and the rVV10 non-local dispersion model of Sabatini *et al*.[2] We modified the non-dimensional *b* and *c* parameters according to the reparameterization of Ning *et al*.[3] (*i.e.*, b = 11.95, and c = 0.0093). The r^{2}SCAN+rVV10 theoretical level provides very accurate results in zeolites.[4] We used the VASP program (version 6.4.3) with the projector augmented-wave method,[5] to perform periodic framework optimizations of the structures. We have used a 2 × 2 × 2 mesh using the Monkhorst-Pack, an energy cut-off of 500 eV, and a break condition for the electronic self-consistent-loop of 10^{-6} eV.
2. **GFN2-xTB (electronic structure) method**: We used the DFTB+ (v. 24.1) program to perform energy optimizations using the TB method in systems with periodic boundary conditions (e.g. salt formed by OSDA cation plus F^- anion in vacuum). We have used the xTB program (v. 6.7)[6] to perform the energy optimizations in the cluster-type systems (without periodic boundary conditions, e.g. OSDAs in vacuum). We used the same theoretical level in both kinds of calculations: the GFN2-xTB Hamiltonian.[7]
3. **Polarizable core-shell (classical) method:** The relative stability of the **ISV**, **BEC**, and crystalline intergrowth **ISV/BEC** frameworks with respect to quartz was evaluated using the General Lattice Program (GULP, version 6.1.2)[8] and the Sanders-Leslie-Catlow (SLC) interatomic potential,[9] following the same energy minimisation procedure described by Balestra *et al.*[10]

2. Construction of crystalline materials

Optimization of the Zeolite-OSDA system

The Cy_3MP^+ and Cp_3MP^+ cations were initially optimised at the GFN2-xTB[GBSA(H_2O)] level, using the ANCOPT engine (which stands for Approximate Normal Coordinate OPTimizer)[11] as implemented in the xTB code. Then, we obtained the ensemble of stable and distinguishable conformers for each cation using the CREST code,[12] at the same theoretical level. We found a total of 63 and 342 distinguishable conformers, for the Cy_3MP^+ and Cp_3MP^+, respectively, employing a conformer energy window threshold < 25 kJ mol^{-1}. The molecular entropy,[13] for the Cp_3MP^+ cation was 41.5 J mol^{-1} K^{-1}, while that of the Cy_3MP^+ cation was 3.2 J mol^{-1} K^{-1}. So, despite the former cation is smaller than the later (47 vs. 56 atoms, respectively), its molecular entropy value is significantly larger. This is related to the value of the conformational entropy of the molecule and shows a larger *flexibility* of the Cp_3MP^+ cation. In fact, just a few Cy_3MP^+ conformers (7 out of 63, ca. 10 %) are enough to add up to ~ 90 % of the total population under standard conditions. However, we need a larger ratio of conformers of the Cp_3MP^+ cation (102 out of 342, ca. 30 %) to add up to the same population.

After having identified a representative ensemble of conformers for each cation (ca. 90 % of the total population), we performed Configurational-Bias Monte Carlo simulations in the canonical ensemble (*NVT*-CBMC) to load four cations per unit cell in the **ISV** structure, for both Cy_3MP^+ and for Cp_3MP^+ cations, at 300 K. We allowed exchanged MC-movement among the conformers. We have used the RASPA (v.2) code.[14] We have employed fixed point-charges and Lennard-Jones interactions in the NVT-CBMC.

Once we have constructed an initial configuration of the zeolite-OSDA system, we performed energy optimizations using the GFN2-xTB or the r^{2}SCAN+rVV10 theoretical level (depending on the context in the main text), explained in the previous section.

Generation and optimization of salts and neutral clusters

We have used the CREST code (using the GFN2-xTB[GBSA(H_2O)] theoretical level) to identify the best conformer and its atomic coordinates for the $Cy_3MP^+F^-$ and $Cp_3MP^+F^-$ complexes (neutral clusters) in

implicit solvation using the Quantum Cluster Growth algorithm at 300 K condition.[15] In this procedure, we also obtained the atomic coordinates of other conformers compatible with 300 K. Once we found the best neutral cluster (*i.e.* the energy minimum), we have optimised it in a box of 16 × 16 × 16 Å to obtain the crystal structure. For that purpose, we performed periodic energy optimisations at r^{2}SCAN+rVV10 theoretical level using the VASP code, as described in the previous methods Section. We initially fixed the length and angle cell parameters to mimic vacuum around the molecule. Then, we performed full-flexible optimisation to obtain the final crystal structure.

The final reference structure for Cp_3MP^+ F^- (Figure S13) has the following cell parameters: a = 9.58 Å, b = 8.32 Å, c = 9.17 Å, α = 59.17º, β = 129.08º, γ = 141.35º. From here, we also constructed the reference structure for Cp_3MP^+ OH^- compound by exchanging the F^- anion by the OH^- anion.

Generation and optimization of structures with defects

In order to simulate a realistic defect concentration, it is necessary to use a 2 × 2 × 1 supercell. This cell is too large to use the r^{2}SCAN+rVV10 method. Therefore, the theoretical level GFN2-xTB has been employed. While there are quantitative differences in the stability predictions, the values can be relied upon qualitatively, as they have been validated with the potential SLC and with the DFT r^{2}SCAN+rVV10 (see Table S2). The construction of the structures with defects was conducted in accordance with the methodology outlined in the main text. In order to incorporate the additional cation, a similar approach was employed to that used for the other cations. In addition to the conventional Monte Carlo (MC) moves for the insertion of the extra cation, the reintroduction and reorientation of the four neighbouring cations (in S1 positions) away from the potential location of the new cation (S2 site) was permitted (Figure S14). This was done in order to accommodate the new extra cation and to enhance the acceptance of all Monte Carlo (MC) moves. To facilitate this process, the temperature was reduced to 100 K and the number of MC steps was increased to 10^7.

Estimation of ^{29}Si NMR chemical shift

The ^{29}Si NMR chemical shift (Figure 10 in main text) was estimated from the optimised CIF files using the method of Dawson *et al.*[16] using the software developed by Balestra *et al.*[10]

*Stability and volume of **ISV** zeolites*

Table S1. Comparison of energy difference between different structures and quartz according to type of calculations. The enthalpy for quartz per T-atom is -29.397, -128.80, and -275.02, eV per T-atom, for r^{2}SCAN+rVV10, SLC potential, and GFN2-xTB methods, respectively. The intergrowth ordered structures (IOS) for **ISV**/**BEC** (BAAB and BAAAB) are showed in Figure S7.

	***Δh* above quartz [kJ mol^{-1} per T-atom]**			
Methods	**BEC**	**ISV**	**IOS-BAAB**	**IOS-BAAAB**
r^{2}SCAN+rVV10	16.44	17.08	-	-
Polarizable SLC's potential	9.94	10.46	10.40	10.33
GFN2-xTB	32.98	33.13	33.067	33.067

Table S2. Comparison of formation enthalpies of **ISV** structures according to the type of calculation. We also list the volume difference, $v = 100\ (V/V_0 - 1)$ [%].

Zeolite	r²SCAN+rVV10		GFN2-xTB	
	Δh* [kJ mol^{-1} per T-atom]	***v*** [%]	***Δh**** [kJ mol^{-1} per T-atom]	***v*** [%]
ISV	17.07	0	33.13	0
ISV-Cp_3MP	1.62	-1.41	13.17	-1.57
ISV-Ch_3MP	4.67	1.3	13.81	0.01
ISV-Cp_3MP-1pOH$^-$ (1 defect -OH + Cp_3MP)	-	-	12.43	-0.91
ISV-Cp_3MP-2Cp_3MPOH^-	-	-	22.20	-0.1

Structural Characterization

We have tried to refine the structure of as-made **ISV** against synchrotron data collected in ALBA (the Spanish synchrotron facility, BL04-MSPD, λ = 0.61928 Å) under different space groups, utilizing GSAS-II[17]. Unfortunately, the refinements never converged and the Rietveld plot showed significant misfitting of the patterns. Introduction of an extra cation to keep consistency with CHN, TG and computational results didn't improve the fitting. Several space groups were explored during the refinement attempts (e.g., tetragonal: $P4_2/mmc$ (#131), $P4_2mc$ (#105), P-42c (#112), P4/m (#83), P4 (#75), $P4_2$ (#77), $P4_222$ (#93), P4/mmm (#123), I4/mmm (#139). orthorhombic: Pmam (#51), Pbmm (#51), Pbm2 (#28), Pma2 (#28), $P2_1am$ (#26), $Pb2_1m$ (#26).) Similarly, attempts to perform a Le Bail full profile fitting under those different space groups also failed (see Figure S6). The bad results are attributed to the existence of structural disorder in **ISV** (*Chem. Mater.* 2007, *19,* 1601-1612).[18]

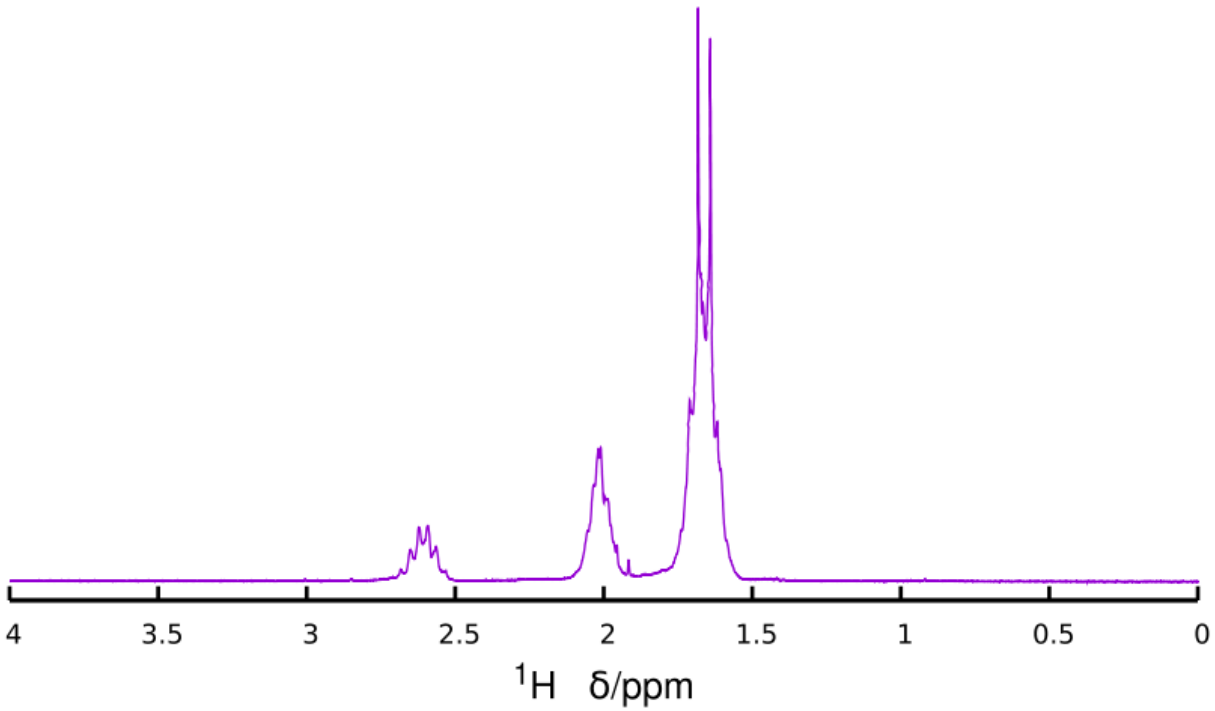

Figure S1. ^{1}H NMR of $Cp_3MP^+I^-$ dissolved in $CDCl_3$ for liquid NMR.

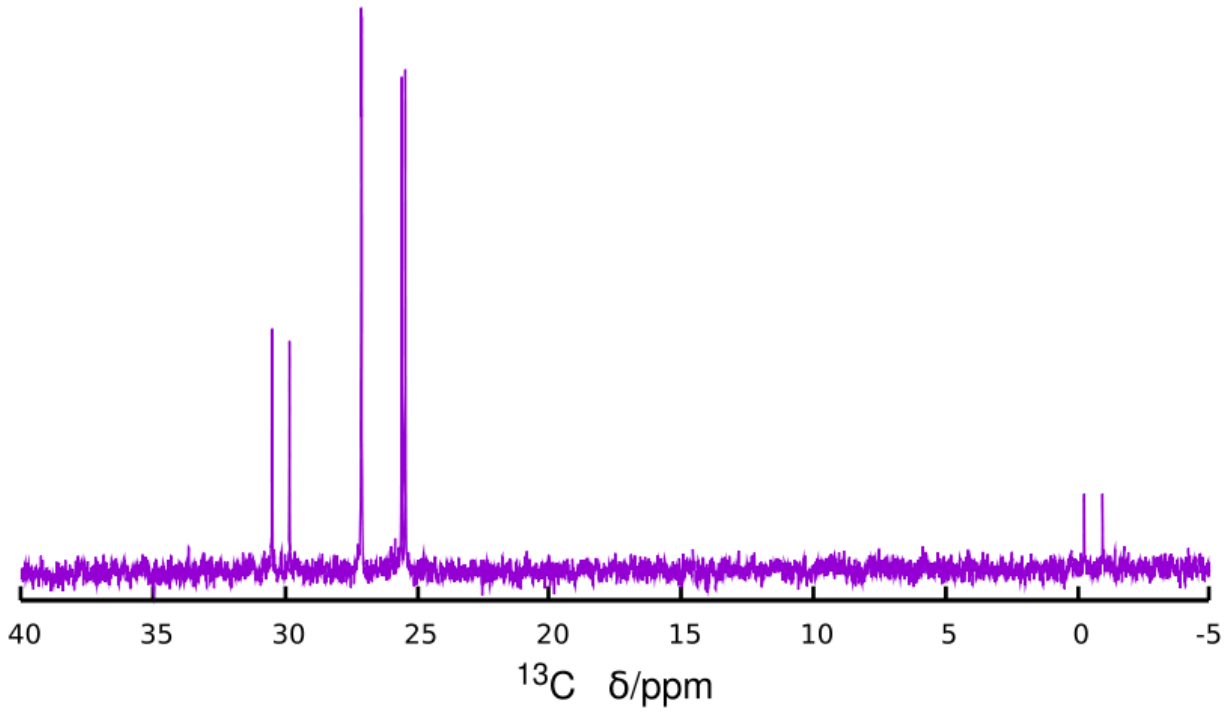

Figure S2. ^{13}C NMR of $Cp_3MP^+I^-$ dissolved in $CDCl_3$ for liquid NMR.

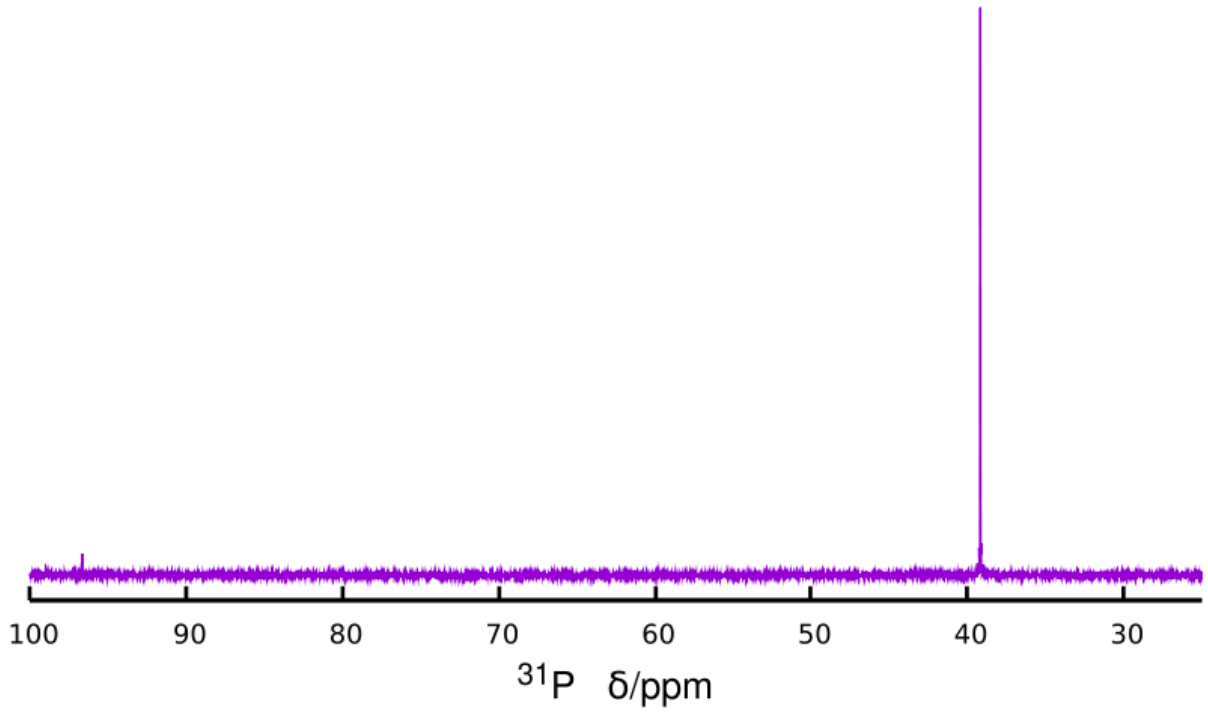

Figure S3. ^{31}P NMR of $Cp_3MP^+I^-$ dissolved in $CDCl_3$ for liquid NMR. The resonance around 97 ppm (<5 % of the total intensity) is attributed to a small impurity in that particular sample.

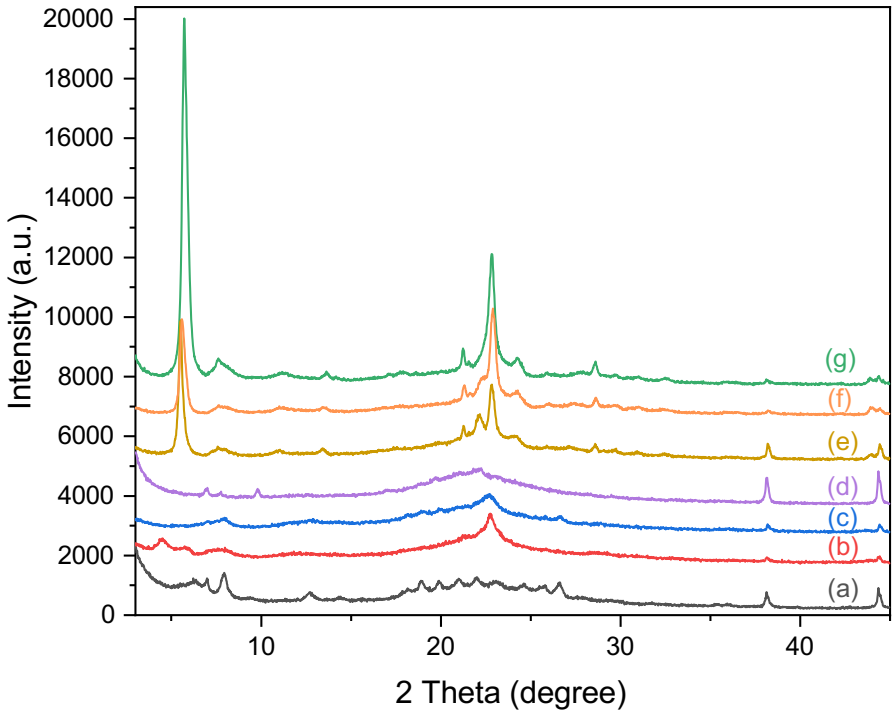

Figure S4. Powder X-ray diffraction patterns of products obtained using Cp_3MP^+ in the nominal absence of HF. IC=Ill-crystallized, UU=Unknown unstable. (a) **IWV**(IC), (b) IC, (c) IC, (d) Am+**ISV**(trace), (e) UU (H_2O/T=15, 190 °C), (f) UU (H_2O/T=10, 175 °C), (g) UU (H_2O/T=10, 190 °C).

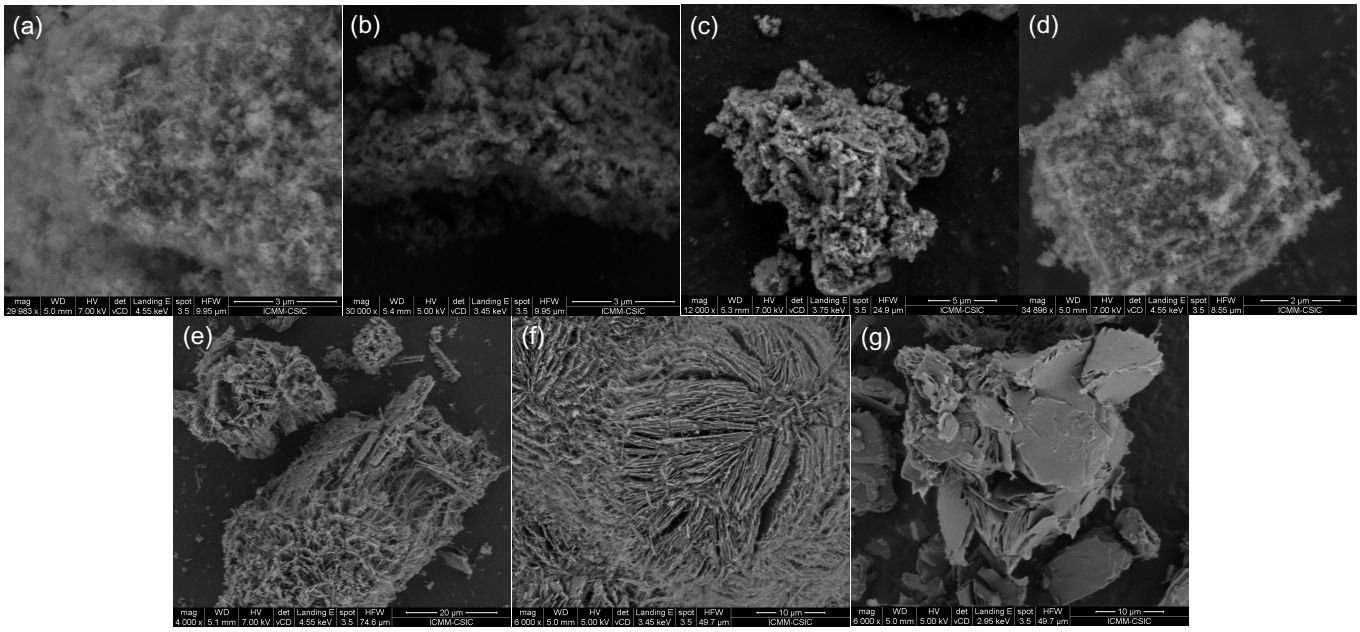

Figure S5. FE-SEM images of products obtained using Cp_3MP^+ in the absence of HF. (a) **IWV**(IC), (b) IC, (c) IC, (d) Am+**ISV**(trace), (e) UU(H_2O/T=15, 190 ℃), (f) UU(H_2O/T=10, 175 ℃), (g) UU(H_2O/T=10, 190 ℃).

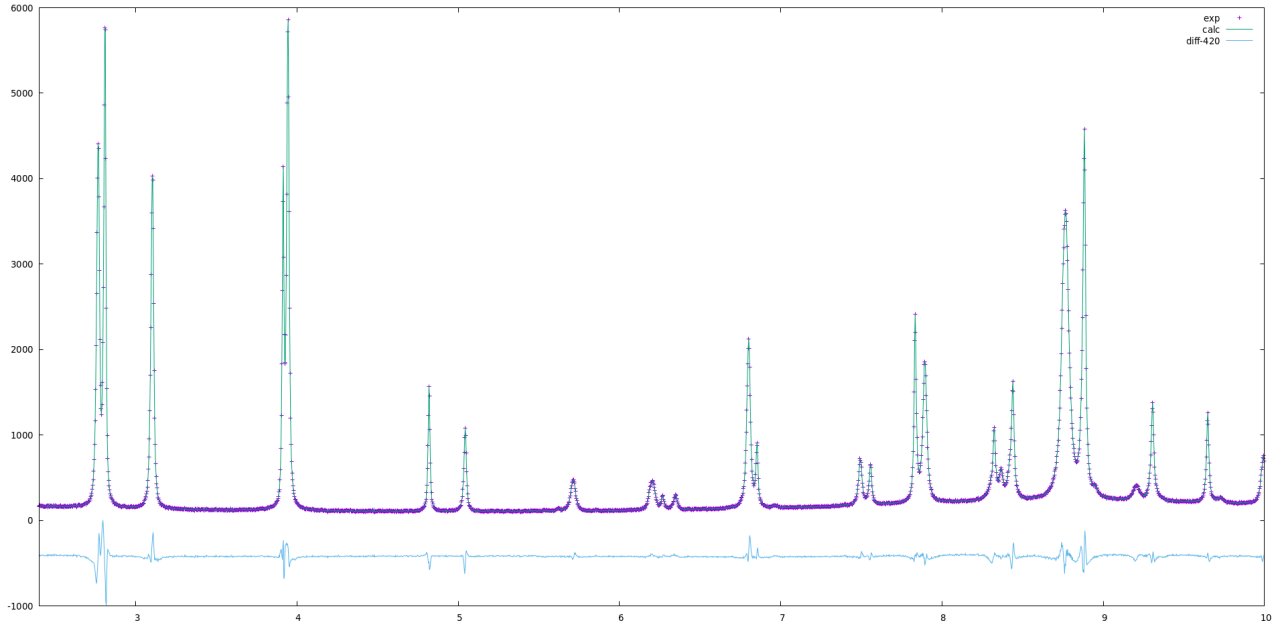

Figure S6. Attempts of full profile fitting of the synchrotron diffraction pattern of **ISV** ($\lambda = 0.61928$ Å) using the Le Bail method failed. Up to 15 different space groups were tried (see above). The best result obtained for space group $P4_2mmc$ is shown in the figure.

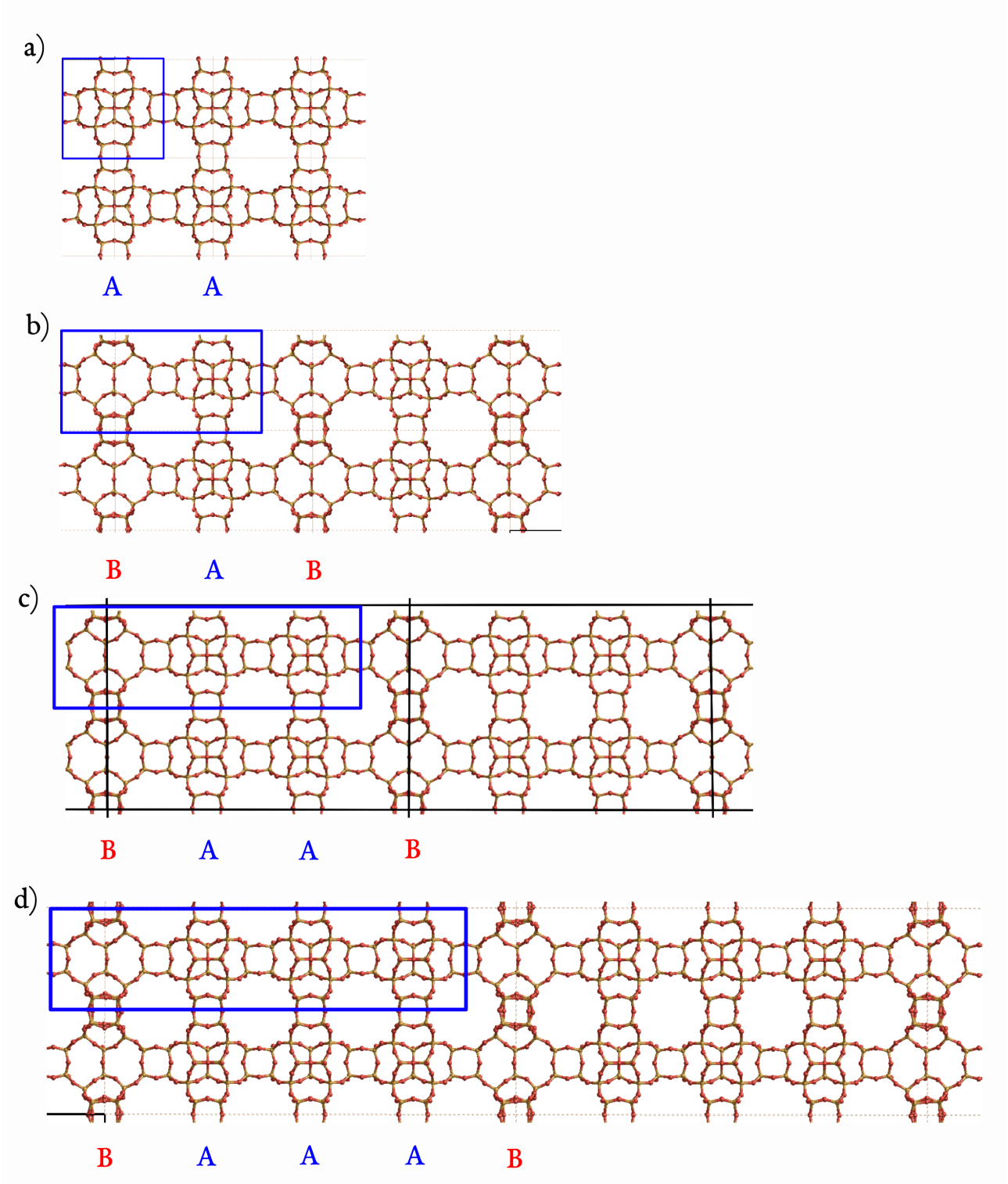

Figure S7. SCL optimised **BEC/ISV** *ordered* intergrowths. a) **BEC** structure (AAA), b) **ISV** (BAB), c) BAAB intergrowth, and d) BAAAB intergrowth. We displayed supercells to visualize more clearly the arrange of layers. The unit cell is highlighted in blue for clarity.

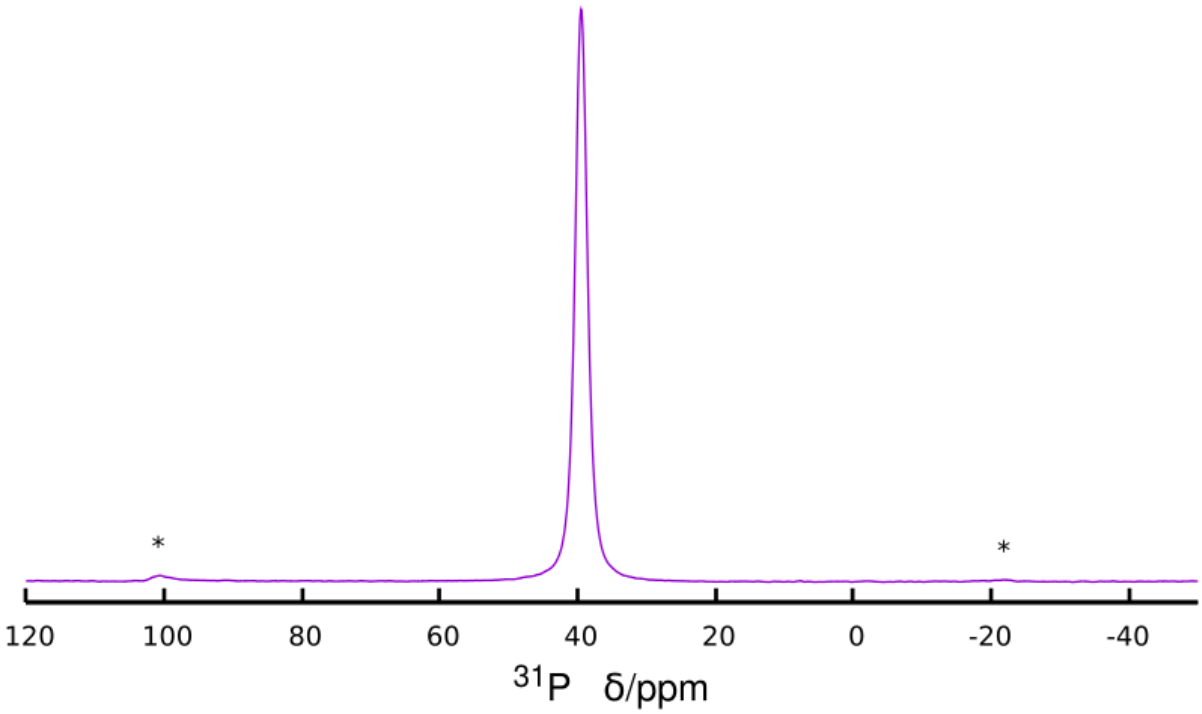

Figure S8. ^{31}P direct irradiation MAS NMR spectrum of CP_3MP-**ISV** zeolite. Spinning side bands are marked with '*'.

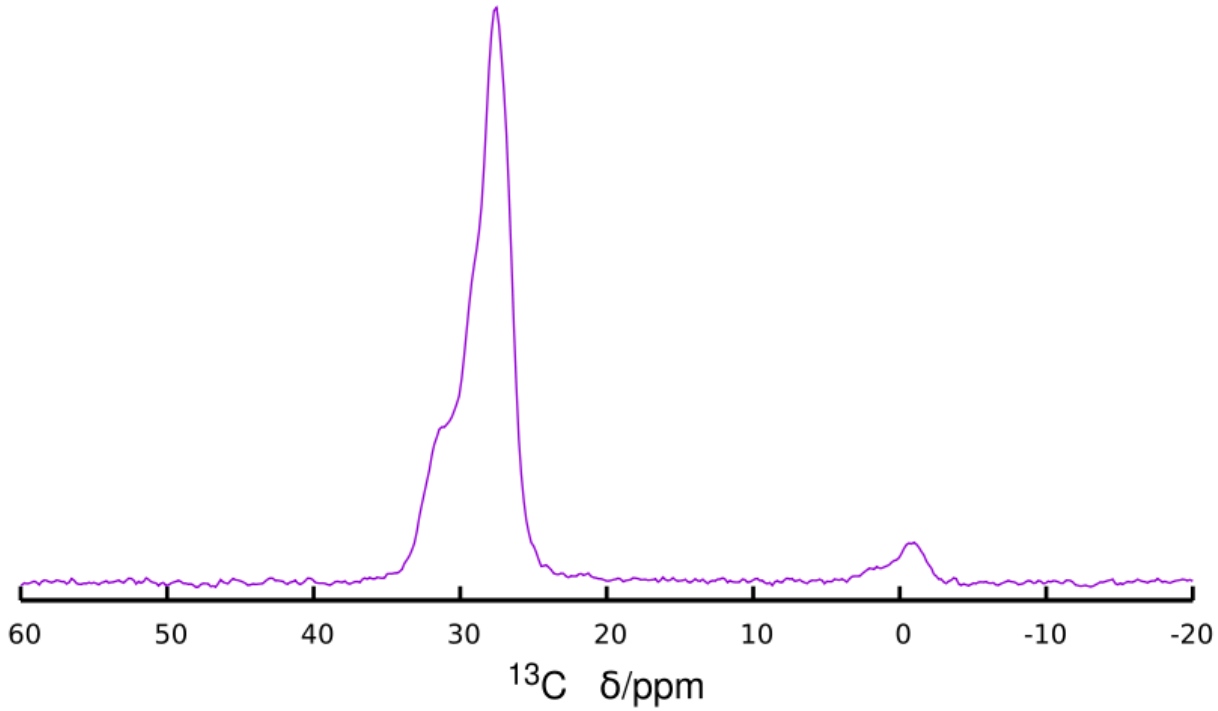

Figure S9. {^{1}H} ^{13}C CPMAS NMR spectrum of CP_3MP-**ISV** zeolite.

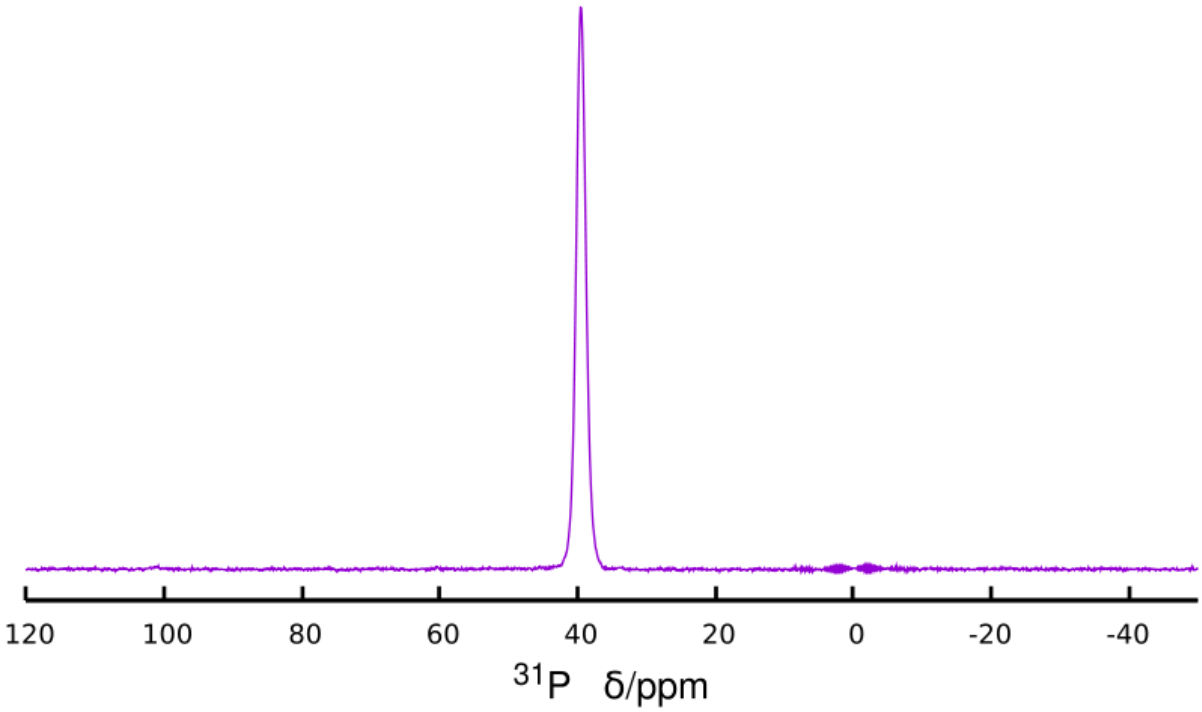

Figure S10. $\{^{1}H\}$ ^{31}P CPMAS NMR spectrum of CP_3MP-**ISV** zeolite.

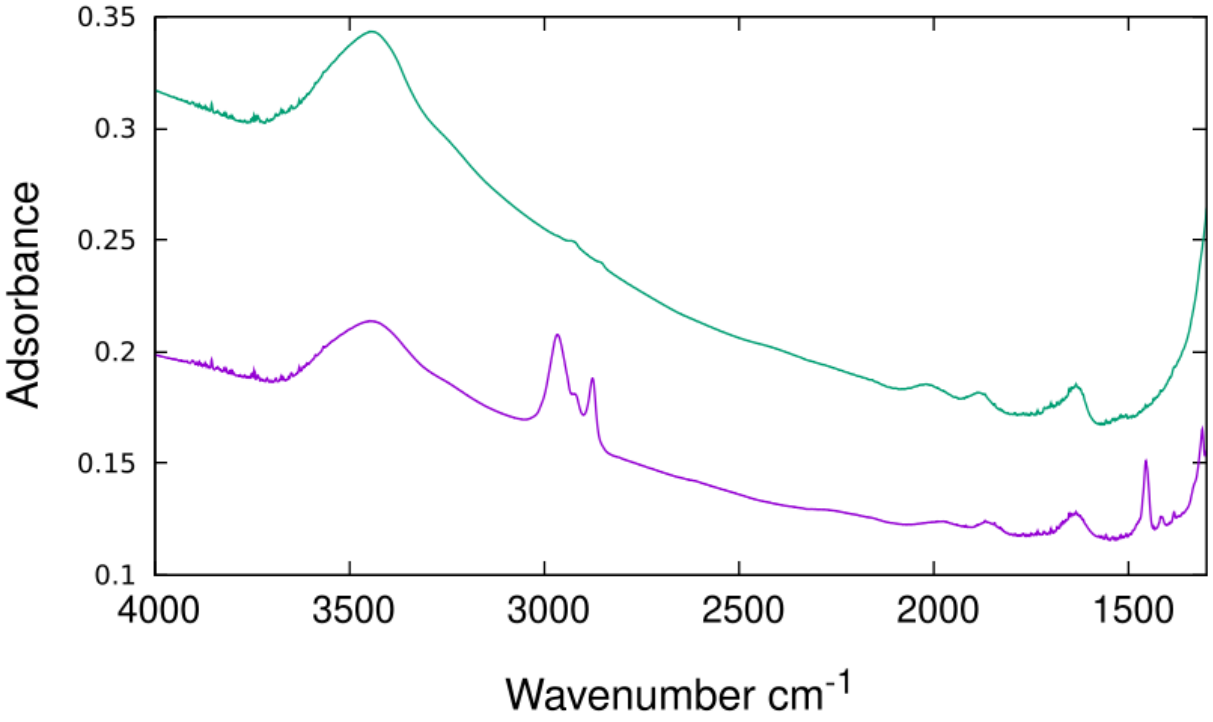

Figure S11. IR spectra in KBr of **ISV** before (bottom) and after calcination, showing the removal of organic moieties. Very small bands at 2925 and 2853 cm^{-1} in the calcined material, which are not coincident with those in the as-made material (2965, 2919 and 2876 cm^{-1}) are assigned to impurities adsorbed in the zeolite from the atmosphere.

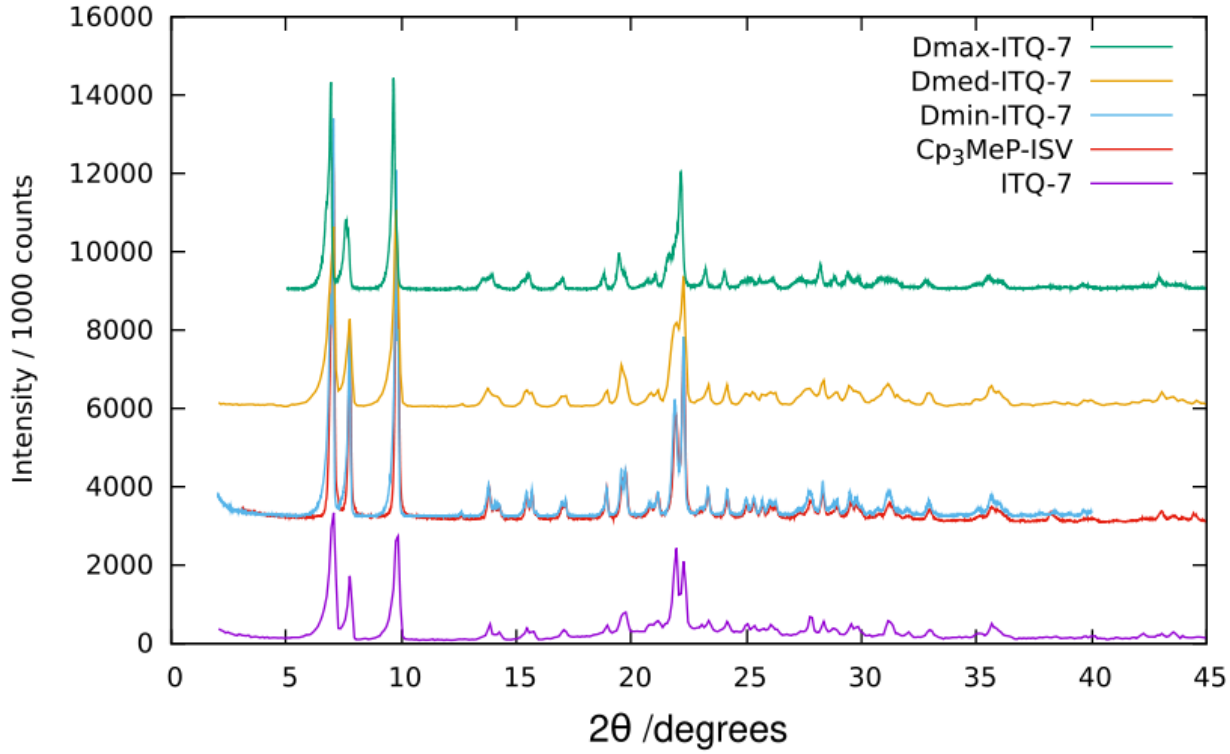

Figure S12. PXRD of Cp_3MP-**ISV** compared to TMATCD-**ISV** with different degrees of disorder. The PXRD of the material reported here is essentially coincident with Dmin-ITQ-7, i.e., a material with moderate disorder. The PXRD data of TMATCD-**ISV** samples were collected by L. A. Villaescusa (Universitat Politécnica de València, Spain).

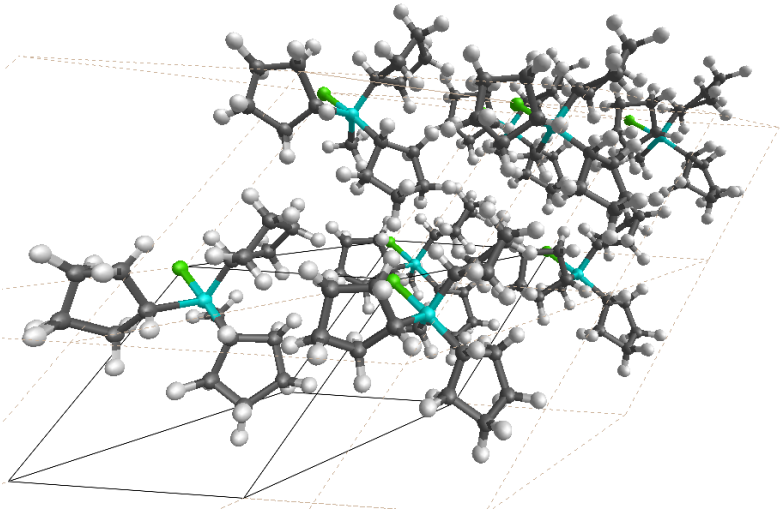

Figure S13. The unit cell of the optimized hypothetical $Cp_3MP^+F^-$ salt.

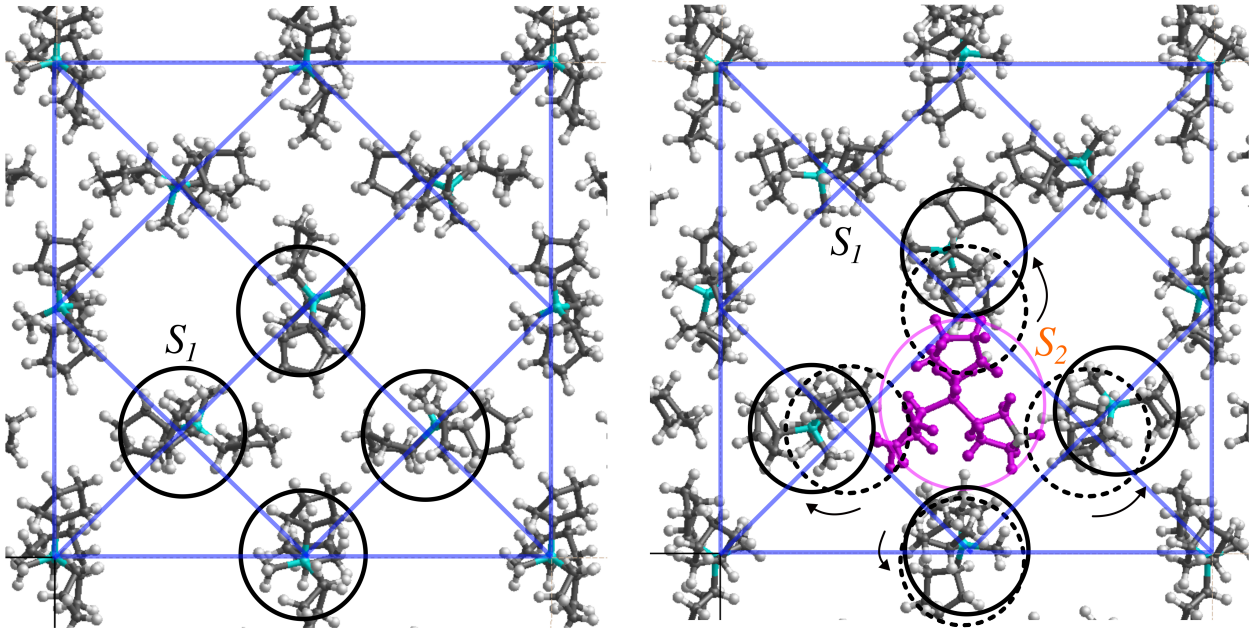

Figure S14. Location of the cations in the **ISV** zeolite (2 x 2 x 1 cell). The zeolite framework and F have been omitted for clarity. The optimized location of 4 cations per unit cell in site S1 is shown at the left. The introduction of defects in the framework allow the introduction of an additional cation at site S2 (purple), with displacement of the nearby cations at S1 as shown in the right figure.

1. J. W. Furness, A. D. Kaplan, J. Ning, J. P. Perdew and J. Sun, *J. Phys. Chem. Lett.*, 2020, **11**, 8208-8215.
2. R. Sabatini, T. Gorni and S. d. Gironcoli, *Phys. Rev. B*, 2013, **87**, 041108.
3. J. Ning, M. Kothakonda, J. W. Furness, A. D. Kaplan, S. Ehlert, J. G. Brandenburg, J. P. Perdew and J. Sun, *Phys. Rev. B*, 2022, **106**, 075422.
4. Z. R. Gao, H. Yu, F.-J. Chen, A. Mayoral, Z. Niu, Z. Niu, X. Li, H. Deng, C. Márquez-Álvarez, H. He, S. Xu, Y. Zhou, J. Xu, H. Xu, W. Fan, S. R. G. Balestra, C. Ma, J. Hao, J. Li, P. Wu, J. Yu and M. A. Camblor, *Nature*, 2024, **628**, 99-103.
5. G. Kresse and J. Furthmüller, *Phys. Rev. B*, 1996, **54**, 11169; G. Kresse and D. Joubert, *Phys. Rev. B*, 1999, **59**, 1758; J. Klimeš, D. R. Bowler and A. Michaelides, *J. Phys.: Condens. Matter*, 2010, **22**, 022201; J. Klimeš, D. R. Bowler and A. Michaelides, *Phys. Rev. B*, 2011, **83**, 195131.
6. C. Bannwarth, E. Caldeweyher, S. Ehlert, A. Hansen, P. Pracht, J. Seibert, S. Spicher and S. Grimme, *WIREs Comput. Mol. Sci.*, 2021, **11**, e1493.
7. C. Bannwarth, S. Ehlert and S. Grimme, *J. Chem. Theory Comput.*, 2019, **15**, 1652-1671.
8. J. D. Gale, *J. Chem. Soc., Faraday Trans.*, 1997, **93**, 629-637; J. D. Gale and A. L. Rohl, *Mol. Simul.*, 2003, **29**, 291-341.
9. M. J. Sanders, M. Leslie and C. R. A. Catlow, *J. Chem. Soc., Chem. Commun.*, 1984, 1271-1273; K.-P. Schröder, J. Sauer, M. Leslie, C. Richard, A. Catlow and J. M. Thomas, *Chem. Phys. Lett.*, 1992, **188**, 320-325; J. D. Gale and N. J. Henson, *J. Chem. Soc., Faraday Trans.*, 1994, **90**, 3175-3179.
10. S. R. G. Balestra, N. Rodríguez-Sánchez, D. Mena-Torres and A. R. Ruiz-Salvador, *Cryst. Growth Des.*, 2024, **24**, 938-946.
11. S. Grimme, ANCOPT: Approximate Normal Coordinate Rational Function Optimization Program, Universität Bonn, Bonn, Germany, 2013; A. Banerjee, N. Adams, J. Simons and R. Shepard, *J. Phys. Chem.*, 1985, **89**, 52-57; J. Baker, *J. Comput. Chem.*, 1986, **7**, 385-395; F. Eckert, P. Pulay and H.-J. Werner, *J. Comput. Chem.*, 1997, **18**, 1473-1483.
12. P. Pracht, S. Grimme, C. Bannwarth, F. Bohle, S. Ehlert, G. Feldmann, J. Gorges, M. Müller, T. Neudecker, C. Plett, S. Spicher, P. Steinbach, P. A. Wesołowski and F. Zeller, *J. Chem. Phys.*, 2024, **160**, 114110.
13. P. Pracht and S. Grimme, *Chem. Sci.*, 2021, **12**, 6551-6568.
14. D. Dubbeldam, S. Calero, D. E. Ellis and R. Q. Snurr, *Mol. Simul.*, 2015, **42**, 81-101.
15. S. Spicher, C. Plett, P. Pracht, A. Hansen and S. Grimme, *J. Chem. Theory Comput.*, 2022, **18**, 3174-3189.
16. D. M. Dawson, R. F. Moran and S. E. Ashbrook, *J. Phys. Chem. C*, 2017, **121**, 15198–15210.
17. B. H. Toby and R. B. Dreele, *J. Appl. Crystallogr.*, 2013, **46**, 544-549.
18. L. A. Villaescusa, I. Díaz, P. A. Barrett, S. Nair, J. M. LLoris-Cormano, R. Martínez-Mañez, M. Tsapatsis, Z. Liu, O. Terasaki and M. A. Camblor, *Chem. Mater.*, 2007, **19**, 1601-1612.